INSTITUTE OF PHYSICS PUBLISHING PHYSICS IN MEDICINE AND BIOLOGY

Phys. Med. Biol. **47** (2002) 2863–2877 PII: S0031-9155(02)29965-0

Monte Carlo modelling of the spectral reflectance of the human eye

S J Preece and E Claridge

Department of Computer Science, University of Birmingham, Birmingham B15 2TT, UK

Received 24 October 2001, in final form 1 May 2002
Published 24 July 2002
Online at stacks.iop.org/PMB/47/2863

Abstract

The interpretation of *in vivo* spectral reflectance measurements of the ocular fundus requires an accurate model of radiation transport within the eye. As well as considering the scattering and absorption processes, it is also necessary to account for appropriate histological variation. This variation results in experimentally measured spectra which vary, both with position in the eye, and between individuals. In this paper the results of a Monte Carlo simulation are presented. Three histological variables are considered: the RPE melanin concentration, the choriodal haemoglobin concentration and the choroidal melanin concentration. By considering these three variables, it is possible to generate model spectra which agree well with *in vivo* experimental measurements of the nasal fundus. The model has implications for the problem of extracting histological parameters from spectral reflectance measurements. These implications are discussed and a novel approach to interpretation of images of the ocular fundus suggested.

1. Introduction

Interpretation of *in vivo* spectral measurements of the ocular fundus can play a valuable role in the study and diagnosis of many ocular disorders. For example, the spectral analysis of the remitted light has been used for estimating the concentration of ocular melanin (Hunold and Malessa 1974) and obtaining quantitative information on the retinal circulation (Delori 1988). It is also becoming increasingly important as a method for detecting pathological changes which occur as a result of ocular diseases (Kilbride *et al* 1989, Knighton 1995, Schweitzer *et al* 1992).

An understanding of *in vivo* reflectance spectra requires a model of radiation transport within the eye. Such a model was first proposed by van Norren and Tiemeijer (1986). Using an arrangement of absorbers and reflectors they were able to obtain parametrized curves which approximated experimental data. This approach was developed by Delori and Pflibsen (1989) who employed the two-flux Kubelka–Munk theory (Kubelka and Munk 1931) to model the interaction of light with the choroidal layer of the fundus. Again, parametrized curves were

obtained which fitted experimental data. Although both studies were able to fit curves to experimental data, neither is based on a realistic physical model of radiation transport within the eye. For example, the Kubelka–Munk theory employed by Delori and Pflibsen requires the incident radiation to be diffuse and the scattering to be isotropic. Neither of these conditions is fulfilled in ocular tissues.

Any model, which is to predict the remitted spectrum from a given biological tissue, must take into consideration the absorption and the scattering processes that occur within each layer. An appropriate solution of the general radiative transport equation must then be obtained at discrete wavelengths. Hammer *et al* (1995) used an inverse Monte Carlo method, with a double-integrating-sphere technique, to obtain the appropriate optical parameters for each of the different layers of the ocular fundus. These parameters were then used in a forward Monte Carlo simulation to predict the *in vivo* reflectance spectrum of a human subject. Their results agreed well with the experimental data.

The remittance spectrum of the ocular fundus varies both with position, in an individual fundus, and between different fundi. This variation is known to result from varying amounts of ocular pigments (Delori and Pflibsen 1989, Weiter *et al* 1986). If the concentration of each pigment is varied through an appropriate physiological range, a suitable model of light transport can compute all possible remittance spectra and hence every possible observed colour. A relationship can then be established between pigment concentration and tissue colour. Once established, this relationship is intended to be used as a part of a novel image interpretation method (Cotton and Claridge 1996, Preece and Claridge 2000). In sections 2 and 3 we explain in detail the assumptions and model necessary to capture the range of remittance spectra observed from the ocular fundus. In sections 4 and 5 the results of the model are compared to the experimental data of Delori and Pflibsen (1989). Good agreement is obtained for all subjects. In section 6 the inverse problem of extracting histological parameters from spectra is discussed and a novel approach to the interpretation of images of the ocular fundus outlined.

2. Background

Figure 1 shows a typical image of the ocular fundus as viewed through an ophthalmoscope. The foveal region is positioned centrally, demarcating a lateral subdivision of the fundus into nasal part (towards the nose) and temporal part (towards the temple). The foveal region is darker than its surroundings as it contains an additional pigment, xanthophyll. The optic disc is positioned nasal to the fovea and has a significantly different tissue structure from the rest of the fundus. In this study the model of radiation transport will be restricted to regions outside the disc, where there is a uniform tissue structure.

Figure 2 shows a schematic representation of the internal structure of the eye. After entering via the cornea, light traverses the intra-ocular media, which consists of the lens and the vitreous. Absorption of light in this layer is known to occur primarily due to the lens pigment (van Norren and Vos 1974) which strongly absorbs in the blue region of the visible spectrum. In young subjects, the absorption does not vary significantly between individuals, but after the age of 30, a process of yellowing begins (Pokorny *et al* 1987). This is often attributed to a thickening of the lens. The absorption spectrum of the vitreous is effectively that of water and was argued by van Norren and Vos (1974) to be negligible in comparison with lens absorption. Using their data, the Lambert–Beer law can be employed to account for absorption of light within the intra-ocular media.

Light is reflected at a number of boundaries within the intra-ocular media, such as the lens–vitreous interface, due to a change in the refractive index. Provided that this specularly

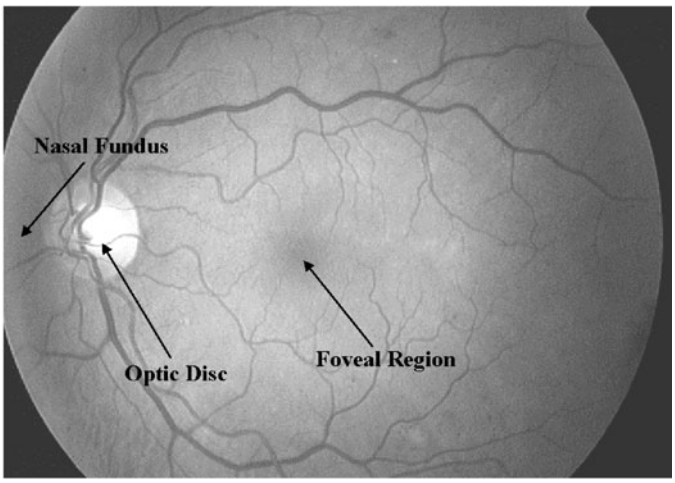

Figure 1. Typical image of the ocular fundus. (Nasal fundus refers to an area nasal of the optic disc.)

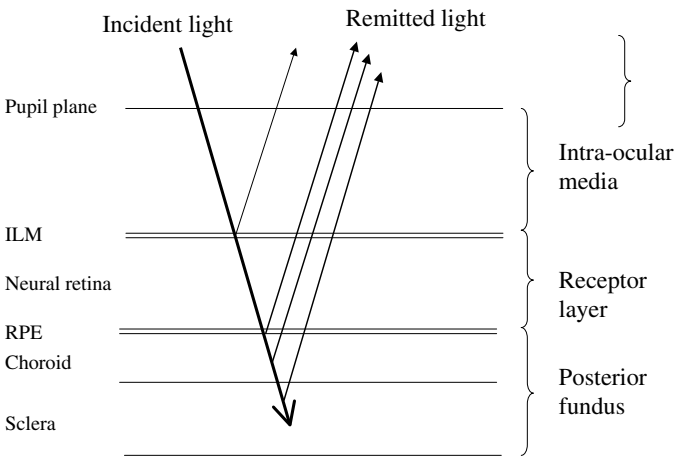

Figure 2. Pathway of light remitted from the ocular fundus.

reflected light does not fall within the collection aperture of the measurement system, the reflections will simply reduce the intensity of the incident light by a wavelength-independent factor. Light passes from the intra-ocular media to the receptor layer via the inner limiting membrane. Although a small fraction of light is reflected at this interface the change in refractive indices is so small (Knighton *et al* 1989) that this fraction can be neglected, typically being less than 1% of light remitted from the poster fundus layers (Gorrand and Delori 1999). The neural retina has a well-defined structure of long slender cells which, because of their small dimensions, can be considered as optical waveguides (Snyder and Pask 1973). In the foveal region of the fundus a directional dependence of the remitted light was observed by van Blockland and van Norren (1986). They proposed a model which explained this directional dependence as a superposition of guided and unguided light. Van de Kraats *et al* (1996) suggested that the directional component results from reflections from the discs containing the visual pigment. This paper will deal with spectroscopic measurements taken after the visual pigment has been bleached. Thus, the directional component of reflection can be neglected.

Despite the regular structure of the neural retina, Hammer *et al* (1995, 2001) showed that the interaction of light with this layer could be modelled with a Monte Carlo technique.

After passing through the receptor layer, light enters the posterior fundus. This comprises three layers: the retinal pigment epithelium (RPE), the choroid and the sclera. Many studies, for example, van Norren and Tiemeijer (1986), have modelled the RPE using the Lambert–Beer law, neglecting the scattering effects. In contrast, Hammer *et al* (1995) measured the optical properties of this layer and found a significant scattering component. By studying the interference pattern under a microscope Bulow 1968 concluded that the scattering took place at the pigment granules which are 0.5–1 μm (Ham 1975). The concentration of RPE melanin is known to vary with position in the fundus and between individuals (Weiter *et al* 1986). This histological variation must be taken into account in any model which is to capture the range of spectral characteristics of the fundus.

The choriod was also shown by Hammer *et al* (1995) to display pronounced scattering characteristics due to the underlying tissue structure and thus must be modelled taking into account anisotropic scatter. In this layer there are a number of pigments, the concentration of which influence the shape of the final remitted spectrum. The first, melanin, has been shown to vary between racial groups and with eye colour (Delori and Pflibsen 1989). The latter variation can be explained by the fact that the choroid is part of the same anatomical layer that comprises the iris. The other pigments are haemoglobin derivatives. The capillary structure of the choroid will give rise to variations in haemoglobin concentration, which, as well as the variations in melanin concentration, must be taken into account.

The final layer is the sclera. This is known to backscatter approximately 50% of incident radiation (Hammer *et al* 1995), the fraction being approximately constant with wavelength giving rise to its white appearance. The posterior fundus is often thought of as a series of absorbers in front of a spectrally neutral reflector, the sclera. The results presented in section 5 illustrate that this is not the case as only a small fraction of the remitted radiation is reflected by the sclera, the vast majority being backscattered in the choroidal layer.

3. Method

Systems developed to measure the spectral reflectance of the ocular fundus consist of an illumination and a collection aperture positioned in the pupil plane. The solid angle subtended by the collection aperture is small, typically about 0.015 steradians; thus the fraction of photons scattered into this aperture, after interacting with the ocular fundus, will also be small. To account for this loss, experimental studies normally report equivalent reflectance. This is obtained by calibrating the measured reflectance spectra against a spectrally neutral reflector placed in the fundus plane. This reflector is always positioned at the same distance from the pupil plane, thus it does not take into account any inter-individual variation in axial length of the eye. To account for such variation it is necessary to introduce a wavelength-independent scaling factor I_0, such that the remitted spectrum is given by

$$I(\lambda) = I_0 f(\lambda).$$

The term $f(\lambda)$ models the shape of the remitted spectrum and is scaled by a factor I_0. These two terms are now considered separately.

3.1. Wavelength-dependent intensity factors

The four-layer model of the fundus requires a model of radiation transport that captures appropriate scattering and absorption. This can be characterized by an absorption coefficient,

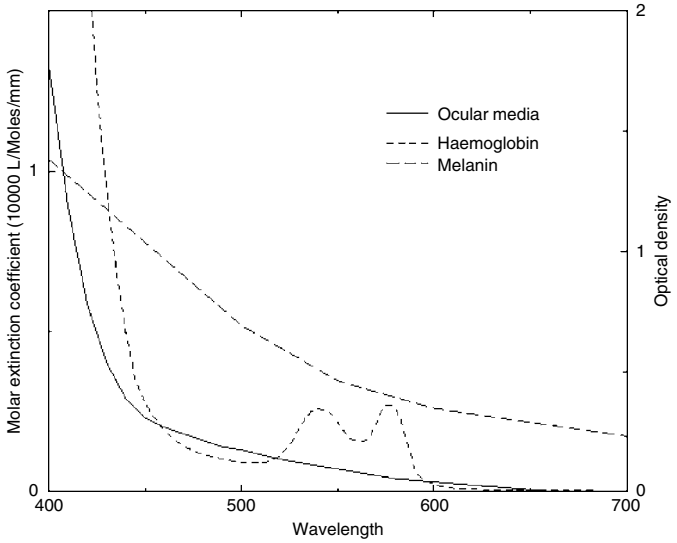

Figure 3. Specific extinction coefficient for melanin and haemoglobin and optical density of the intra-ocular media. The melanin coefficient was taken from Anderson and Parrish (1981), the haemoglobin coefficient from Horecker (1942) and the intra-ocular media density from van Norren and Vos (1974).

μ_a, and a scattering coefficient, μ_s, both of which are a function of wavelength. It is also necessary to take account of anisotropic scatter using an appropriate scattering phase function. For our calculations the Henyey–Greenstein phase function (Henyey and Greenstein 1941) was applied for the description of a single scattering event. This function requires an anisotropy factor, g, which is the mean cosine of the scattering angle and which varies from -1 (backwardly peaked scatter) to 1 (forwardly peaked scatter). Scattering data for each of the four layers was taken from Hammer *et al* (1995). Following the investigation of Hammer and Schweitzer (2002), the scattering coefficient of the neural retina was reduced to 25% of the experimental value published by Hammer *et al* (1995). Experimentally it was only possible to obtain g for larger wavelengths. The remaining values were then estimated assuming g to be constant with wavelength. Other tissue measurements show this to be a valid approximation, g only being observed to vary by a few per cent in the visible range (van Gemert *et al* 1989, Cheong *et al* 1990, Roggan *et al* 1993). The g-values are given as 0.97, 0.84, 0.87 and 0.9 for the neural retina, RPE, choroid and sclera respectively.

As discussed earlier, the characteristics of the remitted spectrum are known to vary with three histological parameters: the RPE melanin concentration, the haemoglobin concentration and the choroidal melanin concentration. Although scattering coefficients were assumed to remain constant with these parameters, absorption coefficients were calculated from a consideration of the three concentrations. Absorption data for the neural retina and sclera were taken from Hammer *et al* (1995) but for the RPE and choroid absorption from the underlying tissue was assumed negligible, all absorption being taken to result from melanin and haemoglobin. In the RPE the absorption coefficient was calculated as the product of the melanin concentration and the specific melanin extinction coefficient, shown in figure 3. In the choroid the absorption coefficient was taken as the sum of that from choroidal melanin and haemoglobin, again using the coefficients in figure 3 and the two respective concentrations.

The absorption spectrum of haemoglobin derivatives in the choroid is essentially that of oxyhaemoglobin (Delori and Pflibsen 1989), thus a 95% oxyhaemoglobin/haemoglobin ratio was taken as representative. These data are taken from Horecker (1942). The specific melanin extinction coefficient was taken from Anderson and Parrish (1981) and can be seen to have the wavelength dependency reported by Gabel *et al* (1978).

Thickness values of 200 μm, 10 μm, 250 μm and 700 μm for the neural retina, RPE, choroid and sclera respectively were taken from Rohen (1977). The Monte Carlo simulation of Prahl *et al* (1989) was then used to obtain the fraction of backscattered light at a number of discrete wavelengths. The mean free path length between two interactions was calculated as $(1/\mu_a + \mu_s,)$ multiplied by the negative logarithm of a random number between zero and one. At each interaction the weight was reduced according to the single particle scattering albedo and the new photon direction calculated using the Henyey–Greenstein phase function. Reflections from boundaries were neglected as no differences in the refractive index have been reported for posterior fundus tissues. Illumination of the fundus is via a small aperture in the pupil plane thus the simulation was performed with collimated incident radiation. Different spot sizes were investigated and, although the fraction of remitted photons collected by a typical aperture varied, the fraction of the remitted photons collected at each wavelength remained constant. An infinitesimal beam simulation was thus used to obtain the final spectrum, any geometrical scaling factor being absorbed into the constant I_0.

Due to the computation expenditure of the Monte Carlo method simulations could only be performed at a limited number of wavelengths. By considering typical experimental spectra the wavelengths 450, 480, 505, 515, 522, 540, 548, 560, 565, 569, 575, 586, 595, 610, 640, 675 and 705 were taken as optimal for reconstruction of the spectral curve. It can be seen from figure 3 that below 450 nm the intra-ocular media absorption is so strong that it renders the remitted spectrum negligible. Thus no simulations were performed below this wavelength. Each spectrum was obtained using typically 100 000 photons. The simulations were performed on a SPARC workstation, each spectrum typically taking 15–30 min. After computation the spectrum was adjusted for a double pass through the anterior ocular media giving the final $f(\lambda)$. The absorption data for the anterior ocular media was taken from van Norren and Vos 1974 and corresponds to subjects between 20 and 30 years old. It must be emphasized that this final $f(\lambda)$ is, in effect, a function of three histological parameters: the RPE melanin concentration, the haemoglobin concentration and the choroidal melanin concentration.

3.2. Wavelength-independent intensity factors

The complex geometrical and optical properties of the eye mean that it is not possible to predict the exact value of I_0 but it is necessary to understand any systematic variation so that inter-individual differences can be accounted for. Reflections occurring in the intra-ocular media constitute a wavelength-independent loss and reflections from the inner limiting membrane can be neglected. Any light remitted from the receptor layer or posterior fundus results from a multiple scattering process, which gradually reverses the photon's direction. Thus, a Lambertian pattern will always be observed. No matter what the scattering and absorption coefficients of each of the layers, the angular distribution of the backscattered light will remain constant and the collection aperture will measure the same fraction of remitted light at all wavelengths. Although wavelength-independent, this fraction will vary with the size of the eyeball. Typically, the eye has an axial length of 22 mm but inter-individual variation of at least ± 1 mm is common and many researchers have reported differences of up to 3 mm (Knighton *et al* 1989). As the intensity of the remitted light at the collection aperture falls

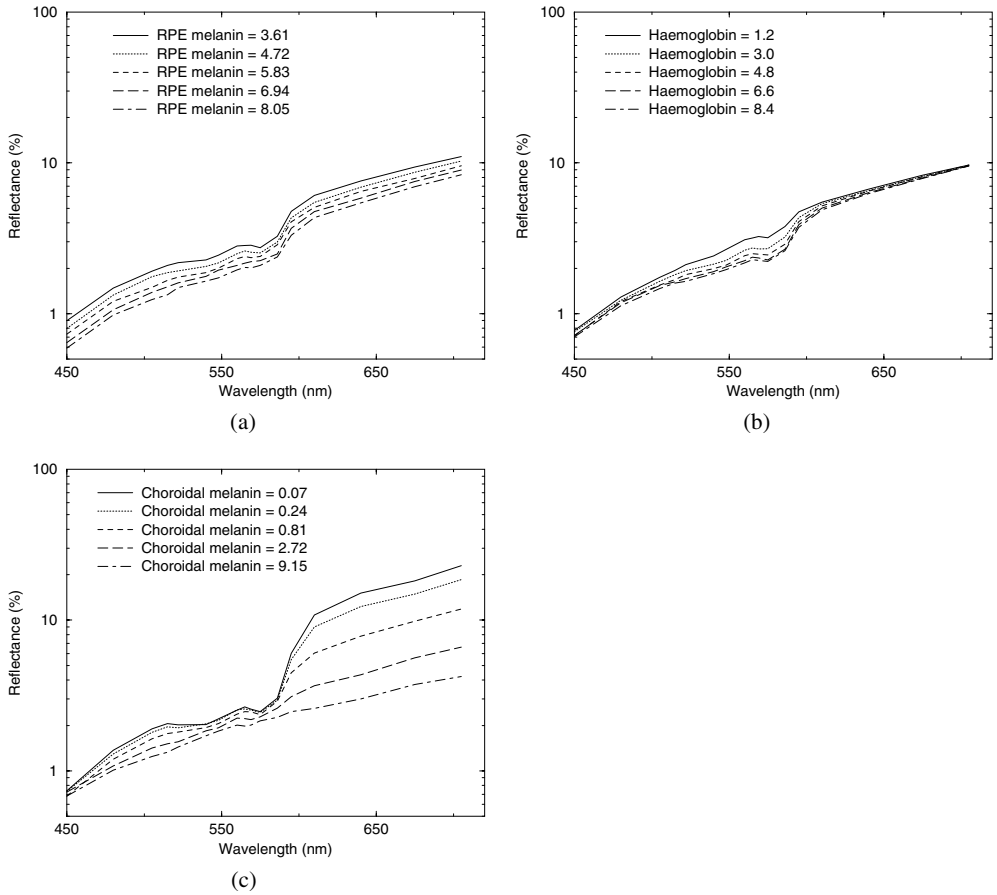

Figure 4. (a) Change in the remitted spectrum as RPE melanin concentration (mmol l^{-1}) is varied with haemoglobin concentration = 5.96 mmol l^{-1} and choroidal melanin concentration = 0.81 mmol l^{-1}. (b) Change in the remitted spectrum as haemoglobin concentration (mmol l^{-1}) is varied with RPE melanin concentration = 5.82 mmol l^{-1} and choroidal melanin concentration = 0.81 mmol l^{-1}. (c) Change in the remitted spectrum as choroidal melanin concentration (mmol l^{-1}) is varied with RPE melanin concentration = 5.82 mmol l^{-1} and haemoglobin concentration = 5.96 mmol l^{-1}.

off with the square of this distance, it is reasonable to expect an inter-individual variation of $\pm 10\%$, corresponding to a 1mm variation in axial length.

4. Results

The model presented above was used to explain the experimentally measured spectra of Delori and Pflibsen (1989). Their data consisted of spectral measurements from three fundus sites of ten subjects, eight Caucasian with varying eye colour, and two non-Caucasian. In this paper, only spectra in the nasal region are analysed as an additional pigment xanthophyll is required to capture spectral variation in other areas of the fundus. Before a fit can is made to the experimental data it is interesting to analyse the effects of the three histological parameters, RPE melanin; haemoglobin and choroidal melanin, on the final remitted spectra. Figures 4(a)–(c) show the effect of varying these parameters through appropriate histological

ranges. The results have been plotted on a log scale to illustrate more clearly changes in the blue and green spectral regions. Increasing the RPE melanin concentration can be seen to have the effect of decreasing the remitted intensity across the whole spectrum. Although initial inspection suggests that this parameter acts as a wavelength independent scaling factor, more careful analysis shows that there is a more pronounced reduction in intensity in the blue than in the red region. This effectively increases the gradient of the whole spectrum. It can also be seen from figure 4(a) that, with an increase in melanin concentration, the oxyhaemoglobin peaks at 540 nm and 576 nm become flattened.

Figure 4(b) shows how the spectrum changes with haemoglobin concentration. Although little effect is observed at the extreme ends of the spectrum there is a significant reduction in intensity in the green region. With an increase in haemoglobin concentration there is an associated flattening of the oxyhaemoglobin peaks and a more rapid increase in intensity at 600 nm. This corresponds to the point at which the oxyhaemoglobin absorption becomes very small, as illustrated in figure 3.

The effect of varying choroidal melanin is shown in figure 4(c). In contrast to the RPE melanin this has a varying effect across the spectrum, the most pronounced change being in the red region. As is commonly accepted, a much larger variation in the remitted spectrum is observed as the choroidal melanin changes through an appropriate histological range. The reduction in intensity beneath 600 nm corresponds to regions where the absorption spectrum of haemoglobin is relatively small. This would be expected as the absorption coefficient is the sum of that from haemoglobin and melanin absorption. The results illustrate the need for a model that not only captures the absorption, but also the scattering characteristics of the ocular fundus. Although the same pigment, melanin, is present in the RPE and the choroid, changing its concentration has a very different effect on the final remitted spectrum. Any diagnostic system, which is required to measure the different pigment concentrations, must take into consideration these differing effects. These ideas are explored further in section 6.

To solve the inverse problem of obtaining the parameters corresponding to a measured experimental spectrum, a simulated evolutionary optimization technique (Fogel 1994, Bäck and Schwefel 1993) was employed. This class of techniques has been described by Yao and Liu (1997) as 'a population-based variant of generate-and-test algorithms. They use search operators such as mutation to generate new solutions and use a selection scheme to test which of the newly generated solutions should survive to the next generation'. The problem of finding histological parameters given a spectral distribution function can be formulated as follows.

Let $I(\boldsymbol{\lambda}) = \{s_1, \ldots, s_w\}$ be a discrete representation of a target spectrum specified at a number of wavelengths $\{\lambda_1, \ldots, \lambda_w\}$. Let $\boldsymbol{x} = \{x_1, \ldots, x_m\}$ be a vector of histological parameters, $\boldsymbol{y} = \{y_1, \ldots, y_w\}$ be a vector representing spectral magnitudes at λ_w, and f: $X \rightarrow Y$ be a function such that $\boldsymbol{y} = f(\boldsymbol{x})$; in this instance f is a Monte Carlo model of light transport.

The objective of optimization is to find a vector of parameters $\boldsymbol{x}_{\min}$ such that the difference between $f(\boldsymbol{x})$ and $I(\boldsymbol{\lambda})$ is minimized:

$$\forall \boldsymbol{x} \quad D(f(\boldsymbol{x}_{\min}),\ I(\boldsymbol{\lambda})) \leqslant D(f(\boldsymbol{x}), I(\boldsymbol{\lambda}))$$

where D is a difference function, also referred to as an 'objective function'; a difference value returned by D is referred to as a 'fitness value' of $\boldsymbol{x}$.

Evolutionary optimization has been implemented by the following algorithm (Yao and Liu 1997):

1. Generate an initial random population of size N, comprising vectors $\boldsymbol{x}^1, \ldots, \boldsymbol{x}^N$ and their associated optimization parameters $\boldsymbol{\eta}^1, \ldots, \boldsymbol{\eta}^N$ (a 'parent' population). Set $k = 1$.

Table 1. The parameters whose values were sought through the optimization process. The lower and upper bounds are used to constrain the values of the initial population in the first step of the optimization.

Parameter	Lower bound	Upper bound
RPE melanin concentration	4.0	7.5
Haemoglobin concentration	0.85	7.0
Choroidal melanin concentration	0	100
Scaling factor	50	62

2. For each vector $\boldsymbol{x}^i$ compute $\boldsymbol{y}^i = f(\boldsymbol{x}^i)$ and evaluate its fitness value according to the objective function D.
3. From each 'parent' pair generate c new pairs $(\boldsymbol{x}, \boldsymbol{\eta})$ of 'offsprings' using the following equations:
$$x_j^{k'} = x_j^i + \eta_j^i N(0, 1) \qquad \eta_j^{k'} = \eta_j^i \exp(\tau' N(0, 1) + \tau N_j(0, 1))$$
where $x_j^{k'}, x_j^i, \eta_j^{k'}$ and η_j^i denote the jth component of the vectors $\boldsymbol{x}^{k'}, \boldsymbol{x}^i, \boldsymbol{\eta}^{k'}$ and $\boldsymbol{\eta}^i$, respectively; $N(0, 1)$ denotes a normally distributed one-dimensional random number with zero mean and standard deviation one. $N_j(0, 1)$ indicates that the random number is generated anew for each value of j. $\tau = (\sqrt{2\sqrt{m}})^{-1}$ and $\tau' = (\sqrt{2m})^{-1}$.
4. For each offspring $\boldsymbol{x}^{k'}$ compute spectrum $\boldsymbol{y}^{k'} = f(\boldsymbol{x}^{k'})$ and evaluate its fitness value using the objective function D.
5. Sort the offsprings $\boldsymbol{x}^{k'}$ according to their fitness value and select the best N offsprings.
6. Replace the original set of vectors $\boldsymbol{x}$ and their associated optimization parameters $\boldsymbol{\eta}$ with the best N pairs selected in step 5.
7. Terminate if the stopping criterion is satisfied; otherwise increment k and go to step 3.

Following a suggestion from a paper by Yao and colleagues (Yao *et al* 1999) step 3 was modified by using two different functions to generate an offspring. Two offsprings were computed first, one using the original Gaussian function $N(0, 1)$, the other one using a one-dimensional Cauchy density function:

$$f_t(x) = \frac{1}{\pi} \frac{t}{t^2 + x^2}.$$

The offspring with a better fitness value was then passed on to step 4.

The algorithm was run for the ten experimentally measured spectra of Delori and Pflibsen (1989) as listed in table 1. Vector $\boldsymbol{x}$ comprised four parameters which are shown in table 1 together with the minimum and maximum values used to generate the initial population in step 1. As discussed in section 3.2 a wavelength-independent scaling factor was included as one of the parameters to account for differences in the axial length of the eye.

The objective function D has a form

$$D(I, y) = \sum_{w=1}^{W} |\log s_w - \log y_w|$$

where $I(\boldsymbol{\lambda}) = \{s_1, \ldots, s_w\}$ is a target spectrum and $\boldsymbol{y} = f(\boldsymbol{x}) = \{y_1, \ldots, y_w\}$ is a spectrum generated by a Monte Carlo simulation from a parameter set $\boldsymbol{x} = \{\boldsymbol{x}_1, \ldots, \boldsymbol{x}_m\}$. Table 2 gives the respective concentrations for each of the pigments along with the appropriate scaling factor for each of the ten experimentally measured nasal fundus curves given in Delori and Pflibsen (1989). Typically, these values were arrived at after 10–20 iterations. The value of the

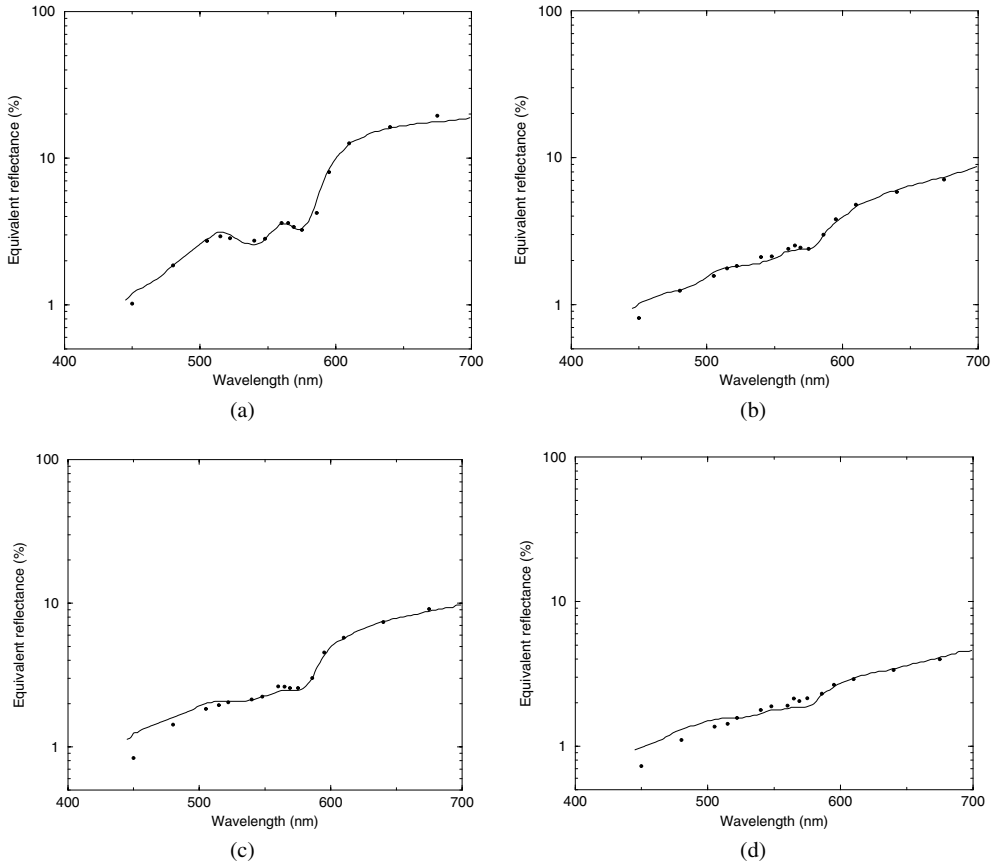

Figure 5. Experimentally measured nasal fundi (solid line) and model predictions (dots) for (a) a Caucasian subject with blue eyes, (b) a Caucasian subject with green eyes, (c) a Caucasian subject with brown eyes and (d) a non-Caucasian subject.

objective function D is a measure of the goodness of fit between the experimentally measured and the computed spectra.

Figures 5(a)–(c) show how the model predictions fit the experimental data for Caucasian subjects with blue, green and brown eyes respectively and figure 5(d) shows the fit for a non-Caucasian subject.

5. Discussion

Although good predictions are seen in figures 5(a)–(d) discrepancies are always observed around $\lambda = 450$ nm and, although not clearly illustrated, in the range just above $\lambda = 700$ nm. The latter discrepancy is due to water in the intra-ocular media which has an absorption peak at 750 nm. At $\lambda = 450$ nm absorption is dominated by the intra-ocular media. A small error in absorption at this wavelength would result in a significant difference in the predicted spectrum. The age range of the subjects in the experimental data reported by Delori and Pflibsen (1989) was 22–38 years, whereas the spectrum was corrected for a double-pass through the intra-ocular media with an absorption which was assumed to be constant with age. As discussed earlier, the lens tends to yellow with age, reducing the absorption in the blue region of the

Table 2. Concentrations of RPE melanin, haemoglobin and choroidal melanin required as input to the model to obtain spectra which fitted the experimentally measured nasal fundus spectra of Delori and Pflibsen (1989). A haemoglobin concentration of 1.7 mmol l^{-1} corresponds to a blood fraction in the choroid of 20% (Hammer and Schweitzer 2002).

Subject	RPE melanin concentration (mmol l^{-1})	Haemoglobin concentration (mmol l^{-1})	Blood fraction	Choroidal melanin concentration (mmol l^{-1})	Scaling factor (I_0)	Fitness function (D)
1	4.53	4.04	47.56	0.22	0.60	0.35
2	6.81	4.96	58.36	0.26	0.59	0.45
3	6.46	5.32	62.56	0.29	0.51	0.93
4	7.06	5.66	66.57	0.23	0.52	0.80
5	5.42	6.18	72.74	1.79	0.56	0.32
6	6.35	6.31	74.18	0.74	0.53	0.76
7	5.29	6.86	80.67	0.76	0.50	0.63
8	4.28	6.96	81.93	1.13	0.53	0.42
9	4.73	6.72	79.10	6.25	0.51	0.58
10	7.29	6.58	77.43	4.26	0.51	1.05

spectrum. To account for this variation it would be necessary to include another histological parameter. It is important to note that the discrepancy at $\lambda = 450$ nm is hardly visible when viewed on a linear scale.

Another possible source of uncertainty in the model is the wavelength dependence of the melanin absorption. Experimental measurements report significantly differing dependencies. For example, Gabel *et al* (1978) and Menon *et al* (1982) report a coefficient which decays like $\lambda^{-4.6}$ at $\lambda = 550$ nm. This is comparable with the functional dependence used for this simulation which was taken from Anderson and Parrish (1981). In contrast, Geeraets *et al* (1962) reported a coefficient which decayed like $\lambda^{-2.2}$. It will be necessary to carry out further experimental study to determine this functional dependence more precisely. Once this has been established it will help to increase the validity of this, and subsequent, models.

Table 2 shows the pigment concentration and overall scaling factor required as input to the model to obtain spectra which match the experimental curves reported by Delori and Pflibsen (1989). As discussed in section 3.2, the differing value of the constant I_0 reflects the changes in the axial length of the eye, which will influence the intensity of the remitted spectrum. A correlation analysis between all four variables showed that there was no significant correlation at the 5% level according to Pearson's test. Using a similar model Hammer and Schweitzer (2002) found significant correlation between different pigment concentrations, in particular, between melanin in the choroid and haemoglobin. This could have been due to their omission of an intensity-scaling factor. Without this factor, changes in eye geometry would have to be accounted for with change in pigment concentration to obtain a spectrum matching that from the experiment.

The average RPE melanin concentration is 5.82 ± 1.11 mmol l^{-1}. In agreement with experimental observation (Weiter 1986), very little variation is observed in this parameter between individuals. Furthermore, it shows no correlation with eye colour/racial group. Using a Monte Carlo simulation of a single layer of RPE at $\lambda = 500$ nm, the transmission, absorption and reflection were obtained for the mean concentration and one standard deviation on either side. The optical density of this layer was then calculated, using $-\log_{10}$ (transmission), to allow comparison with experimental studies. The mean optical density was 0.22 with a range of 0.17–0.24, corresponding to the range of two standard deviations. These numbers agree well with the experimental data of both Weiter *et al* (1986) and Gabel *et al* (1978), who reported

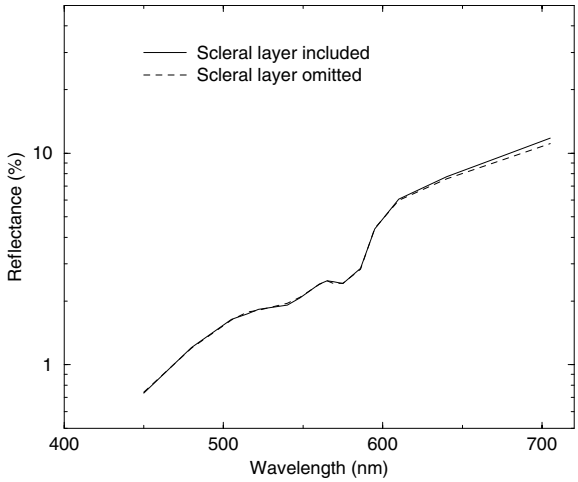

Figure 6. Comparison of predicted remittance spectra with and without the sclera layer for pigment concentration of 5.82 mmol l^{-1}, 5.96 mmol l^{-1} and 0.81 mmol l^{-1} RPE melanin, haemoglobin and choroidal melanin respectively.

similar values for RPE outside the macular region. The reflectance of this layer ranged from 2.1 to 2.7%, again corresponding to a range of two standard deviations. This is slightly higher than the value of 1% reported by Hammer *et al* (1995). This slight disagreement may be due to their overestimation of the absorption coefficient which they subsequently reduced in order to obtain a fit with an *in vivo* experimental measurement of fundus reflectance.

The average value of the haemoglobin concentration is 5.96 $\pm$ 0.95 mmol l^{-1}, which corresponds to a blood fraction in the choroid of 70 $\pm$ 11%. This value is somewhat larger than that found by Hammer and Schweitzer (2002) but, in their study, they found significant correlation between this parameter and choroidal melanin indicating that their value must be interpreted with caution. Delori and Pflibsen (1989) estimated the blood fraction to be about 50% which is in agreement with the experimental results of Lorentz *et al* (1989). In general, the blood fraction in the choriod is taken to range from approximately 30% to70%, which is in agreement with our values.

The choroidal melanin concentration shows the greatest variation and is seen to increase significantly with eye colour/racial group. The average value of 1.59 $\pm$ 2.05 is difficult to compare with experimental studies as absolute concentration has never been reported previously. A calculation of optical density is not informative for this layer, as very little light actually passes through the choroid to the sclera. This is shown in figure 6, which displays model reflectance spectra computed with and without the scleral layer for the average pigment concentrations. It can be seen that there is very little difference in the two remitted spectra. This is because most photons are either backscattered or absorbed in the choroid. Thus, in contrast to what is often believed, light backscattered from the posterior fundus originates primarily from backscatter within the choroidal layer and not from the sclera.

6. Towards model-based interpretation of images of the ocular fundus

Although it has been possible to account for the variation in experimental spectra from a consideration of only three histological parameters, our current model is only valid for young subjects and for the peripheral areas of the fundus. Any model, which is to capture the complete

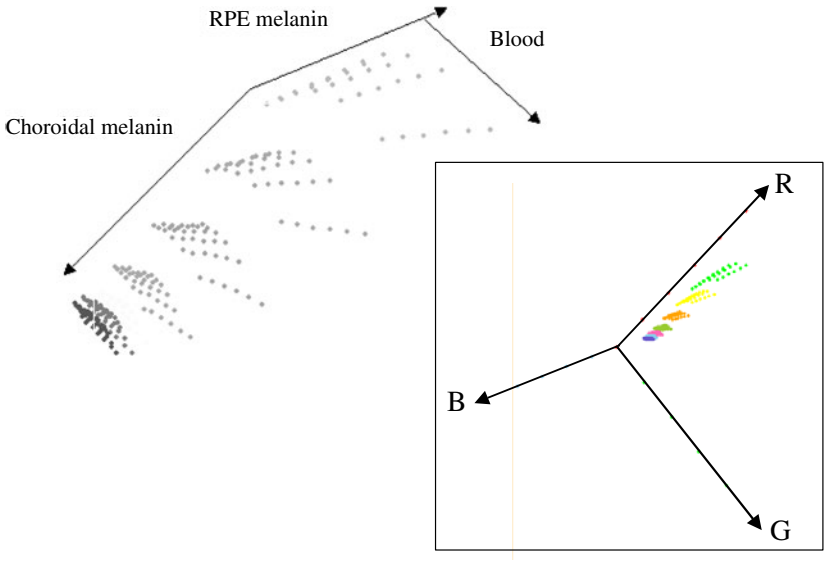

Figure 7. Image values plotted in RGB colour space for a range of values of RPE melanin, haemoglobin and choroidal melanin. In the main figure histological axes have been shown to illustrate the three-dimensional volume mapped out by the set of points. The inset shows the location of colours in RGB space.

(This figure is in colour only in the electronic version)

range of remitted spectra, must take into account all appropriate histological variation. For example, a lens absorption parameter will be required for older subjects and, in the foveal region of the fundus, it will be necessary to model the effect of the macular pigment.

Any system capable of solving the inverse problem of recovering parameter values from experimentally measured spectra would be of major benefit to clinicians. Once recovered, the histological parameters can be used to make an informed diagnosis of any potential ocular abnormalities. Such diagnosis is often based on a comparison of the recovered values and those which are indicative of some pathological condition. Although appropriate in many situations, this approach may lead to confusion due to the large range in pigment concentration found in the fundus. For example, a high concentration of choroidal melanin in a Caucasian subject may indicate the presence of a choroidal nevus, while the same concentration in a non-Caucasian subject may lie within an acceptable range. In this situation it would be preferable to base a diagnosis on parameter values recovered across the whole fundus. Such information could be displayed in the form of a grey-scale image, or parametric map, which would give an ophthalmologist immediate access to the required information for each individual parameter. To produce such a parametric map it is necessary to employ a system capable of measuring and analysing spectral information across the whole fundus. A modified fundus camera has been developed by Schweitzer *et al* (1996) for this purpose. Apart from the economic cost of this system, a major drawback is the time required to analyse spectral information across the whole image. Because of this constraint Schweitzer *et al* (1996) used a highly simplified model of fundus reflectance to recover the parameters of interest. More recently, Hammer and Schweitzer (2002) proposed using the adding–doubling method to obtain model spectra, as this technique is substantially less computationally expensive than a Monte Carlo simulation.

Spectral curves shown in figure 4 were generated by systematically changing one of the three parameters of the optical model of the fundus. Their monotonic behaviour suggests that

the colours which can be observed in fundus images should vary in a similarly systematic way. By convolving the spectra with the appropriate RGB filter response curves, the image values, corresponding to those recorded by a digital fundus camera, can be obtained. In figure 7 image values, computed from the spectra generated from the range of histological variation reported in section 4, have been plotted in the RGB colour space. The RGB axes have been omitted in the main figure to show clearly the appropriate histological variation. The inset shows how the points are distributed if the gain is adjusted equally for each of the R, G and B channels. Clearly, to recover accurate parameter information, it would be necessary to adjust the respective gains to ensure an equal spread of points throughout the colour space. Careful analysis of the RGB data shows that it maps out a 3D volume in colour space. This volume results from the monotonic decrease in image values as pigment concentration is increased. Image values are effectively a weighted positive linear sum of spectral intensities at a number of wavelengths; thus a monotonic decrease in image values will be obtained with an increase in any pigment concentration. This montonicity condition allows extrapolation between points in colour space so that only a relatively small number of image values need to be generated from their corresponding spectra. In figure 7, $6 \times 6 \times 7$ spectra have been used. It is notable that RGB colours associated with the choroidal melanin and the RPE melanin form distinct dimensions in the colour space and therefore can be considered and analysed separately. This monotonic behaviour also indicates that it should be possible to establish a cross-reference between histological quantities and image values for subsequent use in the interpretation of fundus images. Using such cross-reference Cotton and Claridge (1996, 1997) were able to determine the histological parameters of skin from RGB image values. Their work has led to the development of a system which is capable of assisting clinicians in their diagnosis of melanoma (Moncrieff *et al* 2002).

7. Conclusions

A Monte Carlo simulation was employed to predict remitted spectra of the nasal fundus for a range of histological parameters. The model predictions agreed well with experimental observations. The current model is valid for young subjects and specific areas of the fundus but is being developed to account for additional histological variation. It has been shown that the model gives physiologically plausible values for the three histological parameters. This will make it suitable for future use in an image interpretation system for the ocular fundus.

References

Anderson R and Parrish J A 1981 The optics of human skin *J. Invest. Dermatol.* **77** 13–19

Bäck T and Schwefel H-P 1993 An overview of evolutionary algorithms for parameter optimisation *Evol. Comput.* **1** 1–23

Bulow N 1968 Light scattering by pigment epithelium granules in the human retina *Acta Ophthalmol.* **46** 1048–53

Cheong W F, Prahl S A and Welch A J 1990 A review of the optical properties of biological tissue *IEEE J. Quantum Electron.* **26** 2166–85

Cotton S D and Claridge E 1996 Developing a predictive model of human skin colouring *Proc. SPIE* **2708** 814–25

Cotton S D and Claridge E 1997 Noninvasive monitoring skin imaging *Inf. Proc. Med. Imaging* **1230** 501–7

Delori F C 1988 Noninvasive technique for oximetry of blood in retinal vessels *Appl. Opt.* **27** 1113–25

Delori F C and Pflibsen K P 1989 Spectral reflectance of the ocular fundus *Appl. Opt.* **28** 1061–77

Fogel D B 1994 An introduction to simulated evolutionary optimisation *IEEE Trans. Neural Networks* **5** 3–14

Gabel V-P, Birngruber R and Hillenkamp F 1978 Visible and near infrared absorption in pigment epithelium and choroid *Proc. XXIII Consilium Ophthalmologicum* ed K Shimizu and J A Osterhuis (Amsterdam: Experta Medica)

Geeraets W J *et al* 1962 The relative absorption of thermal energy in retina and choroid *Invest. Ophthalmol.* **1** 340

Gorrand J M and Delori F C 1999 Reflectance and curvature of the inner limiting membrane at the foveola *J. Opt. Soc. Am. A* **16** 1229–37

Ham W T 1975 Remarks on fundus reflectance *Vis. Res.* **15** 1167–8

Hammer M and Leistritz L 2001 Light paths in retinal vessel oxymetry *IEEE Trans. Biomed. Eng.* **48** 592–8

Hammer M, Roggan A, Schweitzer D and Muller G 1995 Optical properties of ocular fundus tissue—an *in vitro* study using the double-integrating-sphere technique inverse Monte-Carlo simulation *Phys. Med. Biol.* **40** 963–78

Hammer M and Schweitzer D 2002 Quantitative reflection spectroscopy at the human ocular fundus *Phys. Med. Biol.* **47** 179–91

Henyey L G and Greenstein J L 1941 Diffuse radiation in the galaxy *Astrophy. J.* **93** 70–83

Horecker B L 1942 The absorption spectra of hemoglobin and its derivatives in the visible and near infrared regions *J. Biol. Chem.* **148** 173–83

Hunold W and Malessa P 1974 Spectrophotometric determination of melanin pigmentation of the human ocular fundus *in vivo Opthal. Res.* **6** 355–62

Kilbride P E, Alexander K R, Fishman M and Fishman G A 1989 Human macular pigment assessed by imaging fundus reflectometry *Vis. Res.* **29** 663–74

Knighton R W 1995 Quantitative reflectometry of the ocular fundus *IEEE Eng. Med. Biol.* **14** 43–51

Knighton R W, Jacobson S G and Roman M I 1989 Specular reflection from the surface of the retina *SPIE Laser Surgery: Advanced Characterization, Therapeutics and Systems* **1066** 10–17

Kubelka P and Munk F 1931 Ein Beitrag zur Optik der Farbanstriche *Z. Tech. Opt.* **11** 593–611

Lorentz B, Birngruber R and Vogel A 1989 Quantifizierung der Wellenlangenabhangigkeit laserinduzierter Aderhauteffekte *Fortschr. Ophthalmol.* **86** 644–54

Menon I A, Persad S, Haberman H F, Kurian C J and Basu P K 1982 A qualitative study of the melanins from blue and brown human eyes *Exp. Eye Res.* **34** 531–7

Moncrieff M, Cotton S, Claridge E and Hall P 2002 Spectrophotometric intracutaneous analysis: a new technique for imaging pigmented skin lesions *Br. J. Dermatol.* **146** 448–57

Pokorny J, Smith V C and Lutze M 1987 Aging of the human lens *Appl. Opt.* **26** 1437–40

Prahl S A, Keijzer M, Jacques S L and Welch A J 1989 A Monte Carlo model of light propagation in tissue *SPIE Institute Series IS* **5** 102–11

Preece S J and Claridge E 2000 Physics based medial image understanding of the colouration of the ocular fundus with application to the diagnosis of diabetic retinopathy *Medical Image Understanding and Analysis 2000 (University College London)*

Roggan A, Minet O, Schroder C and Muller G 1993 Measurements of optical tissue properties using integrating sphere technique *SPIE Institute of Medical Optical Tomography IS 11* (Washington, DC: SPIE) pp 149–65

Rohen J W 1977 Anatomie und Embryologic *Augenheilkunde on Klinik und Praxis* ed J Francois and I Hollwich (Stuttgart: Thieme)

Schweitzer D, Hammer M and Scibor M 1996 Imaging spectrometry in ophthalmology—principles and applications in microcirculation and in investigation of pigments *Ophthal. Res.* **28** 37–44

Schweitzer D, Klien S, Guenther S, Hammer M and Scibor M 1992 Early diagnosis of glaucoma by means of fundus reflectometry *New Trends Ophthalmol.* **7** 241–47

Snyder A W and Pask C 1973 The Stiles–Crawford effect: explanations and consequences *Vis. Res.* **13** 1115–23

van Blockland G J and van Norren D 1986 Intensity and polarization of light scattered at small angles from the human fovea *Vis. Res.* **26** 485–94

van de Kraats J, Berendschot T T J M and van Norren D 1996 The pathways of light measured in fundus reflectometry *Vis. Res.* **36** 2229–47

van Gemert M J C, Jaques S L, Sterenbourg H J C M and Star W M 1989 Skin optics *IEEE Trans. Biomed. Eng.* **36** 1164–54

van Norren D and Vos J J 1974 Spectral transmission of the human ocular media *Vis. Res.* **14** 1237–44

van Norren D and Tiemeijer L F 1986 Spectral reflectance of the human eye *Vis. Res.* **26** 313–20

Weiter J J, Delori F C, Wing G L and Fitch K A 1986 Retinal pigment epithelial lipofuscin and melanin and choroidal melanin in human eyes *Invest. Ophthalmol. Vis. Sci.* **27** 145–52

Yao X and Liu Y 1997 Fast evolution strategies *Control and Cybernetics* **26** 467–96

Yao X, Liu Y and Lin G 1999 Evolutionary programming made faster. *IEEE Trans. Evol. Comput.* **3** 82–102